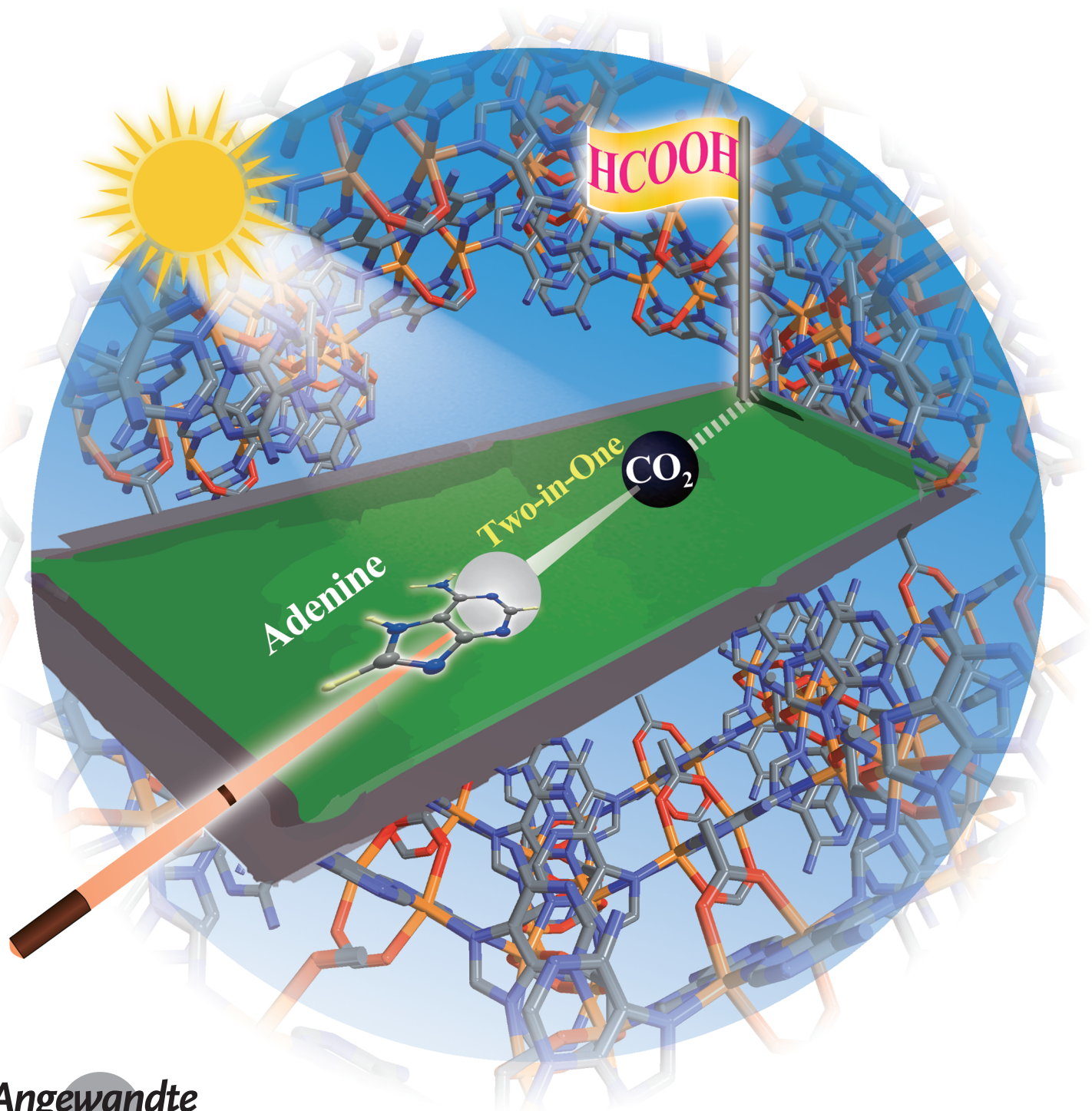


VIP Metal–Organic Frameworks Very Important Paper

International Edition: DOI: 10.1002/anie.201814729
German Edition: DOI: 10.1002/ange.201814729

Adenine Components in Biomimetic Metal–Organic Frameworks for Efficient CO₂ Photoconversion

Ning Li, Jiang Liu, Jing-Jing Liu, Long-Zhang Dong, Zhi-Feng Xin, Yun-Lei Teng, and Ya-Qian Lan*



Abstract: Visible-light driven photoconversion of CO_2 into energy carriers is highly important to the natural carbon balance and sustainable development. Demonstrated here is the adenine-dependent CO_2 photoreduction performance in green biomimetic metal–organic frameworks. Photocatalytic results indicate that **AD-MOF-2** exhibited a very high HCOOH production rate of $443.2 \mu\text{mol g}^{-1} \text{h}^{-1}$ in pure aqueous solution, and is more than two times higher than that of **AD-MOF-1** ($179.0 \mu\text{mol g}^{-1} \text{h}^{-1}$) in acetonitrile solution. Significantly, experimental and theoretical evidence reveal that the CO_2 photoreduction reaction mainly takes place at the aromatic nitrogen atom of adenine molecules through a unique *o*-amino-assisted activation rather than at the metal center. This work not only serves as an important case study for the development of green biomimetic photocatalysts used for artificial photosynthesis, but also proposes a new catalytic strategy for efficient CO_2 photoconversion.

Biological catalysis in nature is an extremely attractive and profound subject because of its eco-friendliness, high-efficiency, and complicated reaction process.^[1] Enzymes as a class of highly sophisticated and powerful biocatalysts are well-known to play the most crucial role in numerous natural reactions.^[2] By some specifically chemical transformations, enzymatic catalysis enables the reaction to occur easily under mild conditions, and is also a longstanding scientific objective for humans.^[3] Of course, the unique catalytic performance of enzymes should be attributed to the synergistic work of multiple components, including active sites, the microenvironment, high substrate affinity, etc.^[4] However, some intrinsic drawbacks, such as poor thermal stability, pH sensitivity, and low tolerance to organic solvents, significantly limit the widespread application of enzymes.^[5] To overcome this dilemma, artificial biomimetic catalysts with enhanced structural robustness but mimicking the beneficial features of enzymes, can facilitate catalytic reactions under harsh reaction conditions.^[6] To date, there are plenty of artificial biomimetic catalysts that have been synthesized and used extensively for some fundamental and complicated catalytic reactions. Moreover, sometimes they show much higher catalytic activity and specificity than the parent biocatalyst.^[7]

In recent years, the increasing anthropogenic CO_2 emissions have resulted in serious energy and environmental issues.^[8] Substantial research efforts are focused on finding effective approaches to realize the conversion of CO_2 .^[9] By imitating the plant photosynthesis, the sunlight-driven artificial CO_2 photoreduction reaction (CO_2RR), converting CO_2



into value-added energy products or chemicals, represents a promising biomimetic conversion pathway.^[10] Considering the intrinsically chemical inertness of CO_2 , the exploration of efficient and stable artificial biocatalysts is regarded as the critical factor of its activation process.^[10b] Furthermore, the accomplishment of CO_2RR s depends largely on the collaborative effect of catalytic active sites, visible-light harvesting, an appropriate microenvironment, CO_2 affinity, etc.^[10b,11] Metal–organic frameworks (MOFs) as an emerging class of porous materials can exhibit enzyme-like advantages for artificial CO_2 photoconversion because they cannot only adsorb and activate CO_2 through open active moieties, but also regulate the light collection and microenvironment of the channel through specifically functionalized organic linkers.^[12] However, only limited MOF-based photocatalysts have been reported for CO_2RR s until now, as most of their structures easily react with H_2O and collapse as a result.^[13] Additionally, toxic organic components in MOFs are also not advisable for green synthesis. In this context, increasing structural robustness and environmental friendliness of MOF-based photocatalysts would thus be a more favorable choice for CO_2RR s.

With these considerations in mind, we focused on the construction of stable and green biomimetic MOFs. Herein, two green biomimetic MOFs, $[\text{Co}_2(\text{HAD})_2(\text{AD})_2(\text{BA})]\cdot\text{DMF}\cdot 2\text{H}_2\text{O}$ (**AD-MOF-1**; HAD = adenine and BA = butanedioic acid) and $[\text{Co}_2(\text{HAD})_2(\text{AD})_2(\text{IA})_2]\cdot\text{DMF}$ (**AD-MOF-2**; IA = isobutyric acid), were obtained under a solvothermal synthesis method. The auxochromic $-\text{NH}_2$ and hydrophobic alkyl groups on the organic linkers make the two MOFs responsive to visible light and show high structural stability.^[14] Furthermore, these biomimetic MOFs are more eco-friendly owing to the use of the nontoxic biological nucleobase adenine and pharmaceutical ingredients. The photocatalytic characterization reveals that **AD-MOF-2** showed a very high HCOOH production rate of $443.2 \mu\text{mol g}^{-1} \text{h}^{-1}$ in an aqueous solution, and is more than two times higher than that of **AD-MOF-1** ($179.0 \mu\text{mol hour}^{-1} \text{g}^{-1}$) in an acetonitrile solution. Significantly, experimental results and theoretical calculations indicate that the CO_2RR mainly occurred at the activated aromatic nitrogen atom of adenine with assistance from the *o*-amino group, and thus represents a new catalytic strategy for efficient CO_2 photoreduction.

Single-crystal X-ray diffraction analysis reveals that **AD-MOF-1** and **AD-MOF-2** crystallize in the same $I4_1/a$ tetragonal space group (see Figure S1 and Table S1 in the Supporting Information) and have very similar asymmetric components composed of one independent Co^{II} ion, one AD^- , and one half of BA^{2-} (**AD-MOF-1**)/one IA^- anion (**AD-MOF-2**). The tetrahedral pyramid coordination geometry of Co^{I} atom in **AD-MOF-1** is comprises two carboxy O and two N atoms from two H_2BA and two HAD ligands, respectively, and one axial N1 atom from another HAD ligand (see Figure S2). Moreover, two nearby Co^{I} atoms constitute a paddle-wheel unit (PWU) by sharing two H_2BA and two HAD ligands (Figure 1a). Analogously, **AD-MOF-2** also exhibits the PWU but with the monocarboxylic HIA instead of dicarboxylic H_2BA (Figure 1b). Each HAD ligand links to three Co^{I} atoms through three aromatic N atoms, the remaining

[*] N. Li, Dr. J. Liu, J.-J. Liu, L.-Z. Dong, Dr. Z.-F. Xin, Prof. Y.-Q. Lan
Jiangsu Collaborative Innovation Centre of Biomedical Functional Materials, Jiangsu Key Laboratory of New Power Batteries, School of Chemistry and Materials Science, Nanjing Normal University
No.1, Wenyuan Road, Nanjing 210023 (China)
E-mail: yqlan@njnu.edu.cn

N. Li, Prof. Y.-L. Teng
School of Chemistry and Chemical Engineering, Yangzhou University
Yangzhou 225002 (P. R. China)

 Supporting information and the ORCID identification number(s) for the author(s) of this article can be found under:
 <https://doi.org/10.1002/anie.201814729>.

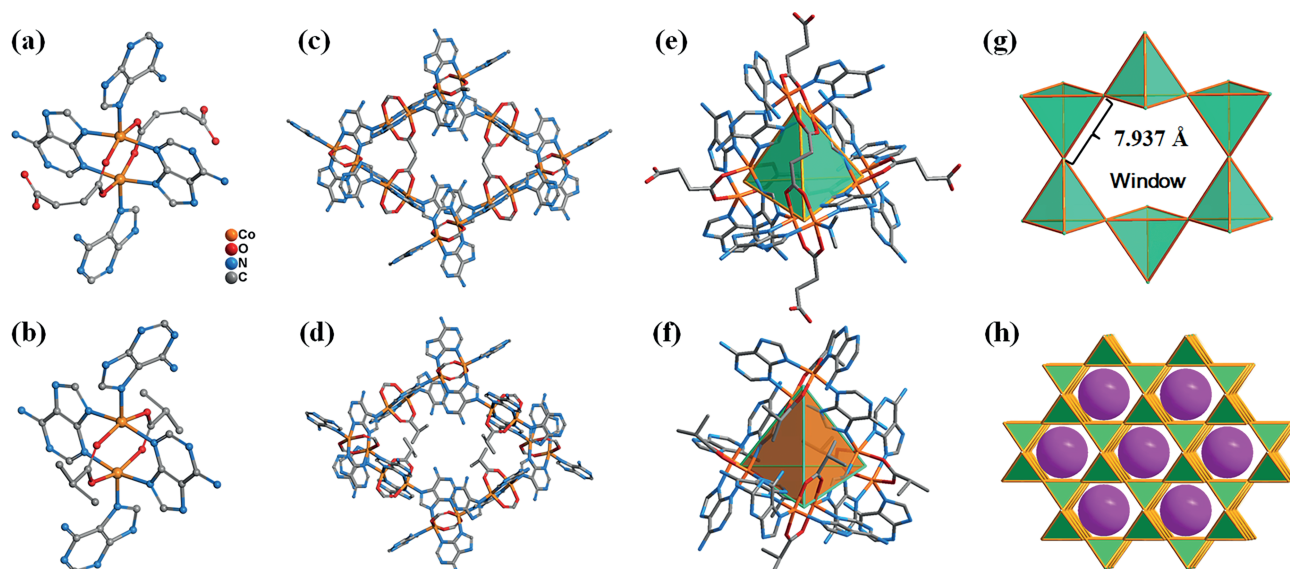


Figure 1. Schematic of the crystal structures of AD-MOFs. a,b) The PWU of **AD-MOF-1** and **AD-MOF-2**. c,d) The hydrophobic alkyl arrangement of either the HIA or H₂BA ligands in the cavities of **AD-MOF-1** and **AD-MOF-2**. e) The regular tetrahedron with PWU as nodes for **AD-MOF-1**. f) The distorted tetrahedron with PWU as nodes for **AD-MOF-2**. Hydrogen atoms are omitted for clarity. g) The PWU with hexagon window in **AD-MOF-1**. h) The 3D microporous network of **AD-MOF-1**.

aromatic and amino N centers are bare (see Figure S2c). The hydrophobic alkyl moieties of HIA or H₂BA ligands uniformly point into the cavities of the MOF networks (Figure 1c,d). Each PWU in **AD-MOF-1** connects six adjacent PWUs through either the N atoms of HAD or carboxy groups of H₂BA and then generates corner-shared and regular PWU-based tetrahedrons (Figure 1e; see Figure S3). In contrast, every PWU in **AD-MOF-2** communicates with four nearby PWUs through the N atoms of the HAD ligands. However, because of the extremely similar structural spatial arrangement, **AD-MOF-2** still shows corner-shared but distorted PWU-based tetrahedrons (Figure 1f; see Figure S3). If the PWU-based tetrahedron is treated as building block, both the **AD-MOFs** can form a three-dimensional microporous network with a classic 6,3 grid-shaped window along the crystallographic *a* axis (Figure 1g,h; see Figure S4).

The phase purity and thermal stability of **AD-MOF-1** and **AD-MOF-2** were confirmed using well-matched powder X-ray diffraction (PXRD) patterns and thermogravimetric analysis (see Figures S5–S7). **AD-MOF-1** is stable in acetonitrile solution, while **AD-MOF-2** remains unchanged in aqueous solution after several days. Furthermore, their structural robustness can also be maintained under traditional photocatalytic conditions for the CO₂RR (see Figures S5 and S6). A broad UV-vis absorption range for **AD-MOF-1** and **AD-MOF-2** revealed that they indeed obtain better light-harvesting abilities by virtue of the auxochromic (–NH₂) decoration on adenine and charge transfer between ligand and metal ion (Figure 2a). Thus the band gaps of 1.76 (**AD-MOF-1**) and 1.52 eV (**AD-MOF-2**) were calculated by the Kubelka-Munk (KM) method (Figure 2b), unveiling their potential to be used as semiconducting photocatalysts.^[12a] Also, Mott–Schottky measurements were performed to determine the LUMO positions of MOFs such that the possible reductive products can be crudely inferred (Fig-

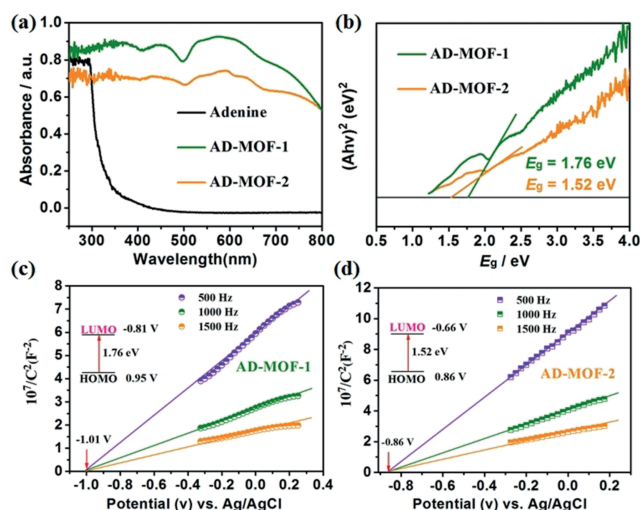


Figure 2. a) UV-vis spectra of adenine, **AD-MOF-1**, and **AD-MOF-2**. b) Tauc plots of **AD-MOF-1** and **AD-MOF-2**. c,d) Mott-Schottky plots for **AD-MOFs** in 0.2 M Na₂SO₄ aqueous solution. Insets are the energy diagrams of the HOMO and LUMO levels of the MOFs.

ure 2c,d). The LUMO locations of the MOFs are more negative than the reduction potentials of many photocatalytic products like HCOOH (0.58 V vs. NHE), CO (0.51 V vs. NHE), etc., indicating that the photogenerated electrons can migrate to the CO₂ molecule for the reduction reaction. Additionally, because adenine is considered an ideal linker, having multiple Lewis-basic sites that can interact with CO₂,^[14b] volumetric CO₂ adsorption measurements were performed on the activated MOF samples at 298 K. As shown in Figure S8a, the CO₂ uptakes of the biomimetic MOFs were determined to be 52.15 and 41.75 cm³ g^{−1}. Besides, the porosity of **AD-MOF-1** and **AD-MOF-2** can

also be demonstrated by their N_2 -adsorption isotherms and pore-size distribution (Figure S8b).

The visible-light-driven CO_2 RR of the activated **AD-MOF-1** (**AD-MOF-2**) was conducted under a pure CO_2 (1.0 atm, 293 K) atmosphere in acetonitrile (aqueous solution) with triisopropanolamine (TIPA) as an electron donor, in the absence of any photosensitizer and noble-metal cocatalysts. $HCOOH$ is the only liquid product detected by ion chromatography (IC; see Figure S9), and no other gaseous products, including competitive H_2 evolution, can be observed by gas chromatography (GC) during the photo-reaction process (see Figure S10). Obviously, these two biomimetic MOFs exhibit highly photocatalytic selectivity for CO_2 reduction. As shown in Figure 3 a,b, the production of

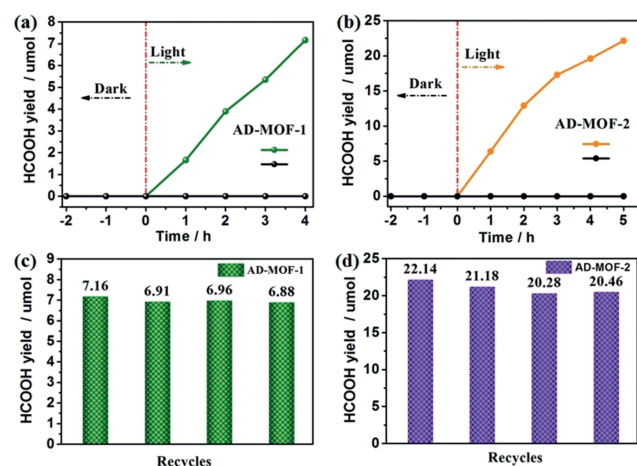


Figure 3. Amounts of $HCOOH$ produced as a function of the time of visible-light irradiation over a) **AD-MOF-1** and b) **AD-MOF-2**. c,d) The recycle experiments were performed by recovering and redispersing the used MOF-based catalyst in a fresh MeCN/ H_2O solution for four/five hours of reaction, showing the photocatalytic durability of the catalyst.

$HCOOH$ for both biomimetic MOFs has a continuous growth as the irradiation time increases. After 4 hours, the maximum $HCOOH$ yield of **AD-MOF-1** reaches up to $7.16 \mu mol$ ($179.0 \mu mol g^{-1} h^{-1}$). By contrast, **AD-MOF-2** shows a higher $HCOOH$ production of $22.16 \mu mol$ ($443.2 \mu mol g^{-1} h^{-1}$) after 5 hours, and is among the highest reported to date (see Table S2).^[12a-c] **AD-MOF-2** has a higher activity than **AD-MOF-1**, and is related to the reduced number of protons in acetonitrile relative to aqueous solution. After the reaction, the MOF-based photocatalysts were removed from the reaction solutions. The leaching of the Co^{II} ions into the resultant filtrate was determined to be 0.062 % (**AD-MOF-1**) and 0.018 % (**AD-MOF-2**) by inductively-coupled plasma analysis. Notably, **AD-MOF-2** is the first green biomimetic MOF applied to the CO_2 RR with H_2O as the reaction solvent, and it is preferable for the practical and feasible green synthesis. Furthermore, nontoxic adenine as photosensitizer is, also for the first time, explored as a substitute for a porphyrin derivative, which is the commonly used visible-light harvesting component for the CO_2 RR.^[10c,12a] To confirm the photocatalytic activity of biomimetic MOFs, a series of

deletional control experiments were conducted in the absence of photocatalysts, CO_2 , or light illumination, and no detectable products were observed by IC and GC in the reaction system (see Table S3). The effects of stoichiometric mixtures of the component raw materials used for the synthesis of **AD-MOF-1** and **AD-MOF-2** were examined under identical photocatalytic conditions. Results revealed that the reductive products are trace amounts of $HCOOH$ and CO (see Table S3), corroborating the potential of biomimetic MOFs for photoconverting CO_2 into $HCOOH$. Also, photoluminescence (PL) emission spectra of **AD-MOF-1** and **AD-MOF-2** before and after the addition of a sacrificial agent were further conducted to investigate the photocatalytic quenching behavior. As shown in Figure S11, the decreased PL intensity of the MOF-based photocatalysts suggest that the photo-excited holes in the photocatalytic CO_2 RR process were significantly consumed by TIPA. The photocatalytic stability was evaluated by recycling experiments, in which the photocatalysts nearly maintained their initial activities even after four cycles (Figure 3c,d). The slight decay of the $HCOOH$ production rate is probably due to the mass loss in the recovery process of the used photocatalysts. The resultant filtrates did not show any obvious UV-vis absorption (see Figure S12), and excludes the influence of the decomposed active components from catalysts on the photocatalytic activity. Importantly, no noticeable changes were observed on IR spectra and PXRD patterns performed before and after CO_2 RR, confirming the heterogeneous nature of biomimetic **AD-MOF-1** and **AD-MOF-2** (see Figures S13 and S14). To validate the carbon source origin of the produced $HCOOH$, the isotopic ^{13}C experiment was performed under identical photocatalytic reaction, and the products were identified by ^{13}C NMR spectroscopy. As shown in Figure S15, the ^{13}C NMR spectrum clearly gives the $HCOOH$ signal, which is consistent with previous work.^[12a-c] These results unambiguously demonstrate that biomimetic MOFs are indeed active for converting CO_2 into $HCOOH$ under visible-light irradiation.

The catalytically active sites of the biomimetic MOFs for CO_2 -to- $HCOOH$ conversion can be identified by their well-defined crystalline structures. It is impractical for the metallic PWU unit in biomimetic MOFs to be the active site because of its saturated coordination sphere. In contrast, the CO_2 photoconversion is more likely to occur at the adenine moiety which has a bare aromatic and amino N, especially considering that some nanostructured N-doped materials or N-heterocyclic carbenes have proven to be active in photocatalysis.^[15]

To gain more insight into the photocatalytic mechanism, DFT calculations related to CO_2 adsorption and activation were carried out to confirm the active sites. Interestingly, the CO_2 molecule can escape quickly when used to attack metallic PWUs (see simulation video in the Supporting Information), consistent with our foregoing speculation, suggesting that the photocatalytic process is unlikely to take place at this segment. In contrast, the CO_2 molecule is more likely to interact with adenine through strong hydrogen bonding at the $-NH_2$ group (Lewis-basic site), and can be clearly demonstrated from the adsorption energy of $*CO_2$ (≈ -0.37 eV). Furthermore, the free energy of the $*COOH$

intermediate structure falls by about 0.63 eV as the first proton-coupled electron transfers to CO₂ on the neighbouring aromatic N atom, thus facilitating the CO₂RR. The free-energy pathway of CO₂-to-HCOOH conversion at the adenine of the biomimetic MOFs and the intermediate architectures are shown in Figure 4a. *HCOOH formation

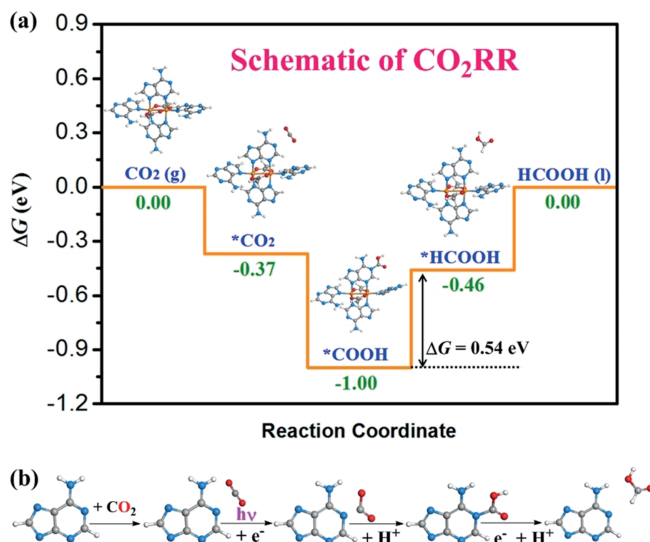


Figure 4. a) Calculated free-energy diagram for CO₂RR based on biomimetic MOFs. b) Simulated CO₂-to-HCOOH conversion reactive pathway over adenine molecule of biomimetic MOFs under visible-light irradiation.

serves as the rate-limiting step ($\Delta G = 0.54$ eV) for the four elementary reaction steps. The overall calculation results indicate that the CO₂RR can readily occur at the bare aromatic N atom of adenine, with the assistance from *o*-amino group, through strong binding with the activated CO₂ intermediate. Additionally, the calculated electron density distribution demonstrated that the density on the HOMO and LUMO orbitals of the MOF structure are principally localized on the adenine molecule (see Figure S19). Therefore, light irradiation can generate photoexcited electrons at adenine where the aromatic N atom serves as the active site for subsequent CO₂-to-HCOOH conversion (Figure 4b). Moreover, an additional verification experiment that adenine and [Ru(bpy)₃]Cl₂·6H₂O (bpy = 2,2'-bipyridine) were used as homogeneous catalyst and auxiliary photosensitizer (PS) to perform identical CO₂RRs, which exhibited a comparable HCOOH production rate of 171.7 μmol hour⁻¹ g⁻¹, further confirming the photocatalytic CO₂-to-HCOOH activity of adenine. In contrast, no HCOOH was produced in the system without PS because of inferior visible-light harvesting of adenine itself. Importantly, heterogeneous biomimetic MOFs have better photocatalytic performance than the homogeneous adenine molecule and is mainly attributed to their synergistic effect of good visible-light harvesting, appropriate microenvironment, and strong CO₂ affinity.

In summary, two green biomimetic MOFs were synthesized and used as photocatalysts for the CO₂RR. AD-MOF-2 exhibited a very high HCOOH production rate in pure

aqueous solution. Significantly, the CO₂RR mainly occurred at the aromatic N atom of adenine with assistance from the *o*-amino group, and presents a new catalytic strategy for efficient CO₂ photoreduction. Additionally, because the employed MOF structures were assembled with eco-friendly components, we hope this work will provide an important step towards the development of more-stable and green biomimetic MOFs for CO₂ photoreduction.

Acknowledgements

This work was financially supported by NSFC (No. 21622104, 21871141, 21871142 and 21701085), the NSF of Jiangsu Province of China (No. SBK2017040708, BK20171032), the Natural Science Research of Jiangsu Higher Education Institutions of China (No. 17KJB150025), Priority Academic Program Development of Jiangsu Higher Education Institutions, and the Foundation of Jiangsu Collaborative Innovation Center of Biomedical Functional Materials.

Conflict of interest

The authors declare no conflict of interest.

Keywords: biomimetic catalysis · hydrophobicity · metal–organic frameworks · photochemistry · photosynthesis

How to cite: *Angew. Chem. Int. Ed.* **2019**, *58*, 5226–5231
Angew. Chem. **2019**, *131*, 5280–5285

- [1] G. Grogan, *Annu. Rep. Prog. Chem. Sect. B* **2013**, *109*, 15–42.
- [2] a) K. M. Koeller, C.-H. Wong, *Nature* **2001**, *409*, 232; b) A. Schmid, J. S. Dordick, B. Hauer, A. Kiener, M. Wubbolts, B. Witholt, *Nature* **2001**, *409*, 258.
- [3] T. J. Schwartz, B. J. O'Neill, B. H. Shanks, J. A. Dumesic, *ACS Catal.* **2014**, *4*, 2060–2069.
- [4] a) X. Lian, Y. Fang, E. Joseph, Q. Wang, J. Li, S. Banerjee, C. Lollar, X. Wang, H.-C. Zhou, *Chem. Soc. Rev.* **2017**, *46*, 3386–3401; b) S. J. Benkovic, S. Hammes-Schiffer, *Science* **2003**, *301*, 1196–1202.
- [5] J.-M. Choi, S.-S. Han, H.-S. Kim, *Biotechnol. Adv.* **2015**, *33*, 1443–1454.
- [6] X. Lian, A. Erazo-Oliveras, J.-P. Pellois, H.-C. Zhou, *Nat. Commun.* **2017**, *8*, 2075.
- [7] a) D. Feng, Z.-Y. Gu, J.-R. Li, H.-L. Jiang, Z. Wei, H.-C. Zhou, *Angew. Chem. Int. Ed.* **2012**, *51*, 10307–10310; *Angew. Chem.* **2012**, *124*, 10453–10456; b) M. Zhao, S. Ou, C.-D. Wu, *Acc. Chem. Res.* **2014**, *47*, 1199–1207.
- [8] a) N. Armadori, V. Balzani, *Angew. Chem. Int. Ed.* **2007**, *46*, 52–66; *Angew. Chem.* **2007**, *119*, 52–67; b) M. Mikkelsen, M. Jørgensen, F. C. Krebs, *Energy Environ. Sci.* **2010**, *3*, 43–81.
- [9] a) T. Sakakura, J.-C. Choi, H. Yasuda, *Chem. Rev.* **2007**, *107*, 2365–2387; b) M. Aresta, A. Dibenedetto, A. Angelini, *Chem. Rev.* **2014**, *114*, 1709–1742.
- [10] a) Y. Zheng, L. Lin, B. Wang, X. Wang, *Angew. Chem. Int. Ed.* **2015**, *54*, 12868–12884; *Angew. Chem.* **2015**, *127*, 13060–13077; b) X. Chang, T. Wang, J. Gong, *Energy Environ. Sci.* **2016**, *9*, 2177–2196; c) H. Rao, L. C. Schmidt, J. Bonin, M. Robert, *Nature* **2017**, *548*, 74–77.

- [11] Y. Wang, Z. Zhang, L. Zhang, Z. Luo, J. Shen, H. Lin, J. Long, J. C. S. Wu, X. Fu, X. Wang, C. Li, *J. Am. Chem. Soc.* **2018**, *140*, 14595–14598.
- [12] a) H.-Q. Xu, J. Hu, D. Wang, Z. Li, Q. Zhang, Y. Luo, S.-H. Yu, H.-L. Jiang, *J. Am. Chem. Soc.* **2015**, *137*, 13440–13443; b) D. Wang, R. Huang, W. Liu, D. Sun, Z. Li, *ACS Catal.* **2014**, *4*, 4254–4260; c) Y. Fu, D. Sun, Y. Chen, R. Huang, Z. Ding, X. Fu, Z. Li, *Angew. Chem. Int. Ed.* **2012**, *51*, 3364–3367; *Angew. Chem.* **2012**, *124*, 3420–3423.
- [13] S. Yuan, L. Feng, K. Wang, J. Pang, M. Bosch, C. Lollar, Y. Sun, J. Qin, X. Yang, P. Zhang, Q. Wang, L. Zou, Y. Zhang, L. Zhang, Y. Fang, J. Li, H. C. Zhou, *Adv. Mater.* **2018**, *30*, 1704303.
- [14] a) J. An, S. J. Geib, N. L. Rosi, *J. Am. Chem. Soc.* **2010**, *132*, 38–39; b) T. Li, D.-L. Chen, J. E. Sullivan, M. T. Kozlowski, J. K. Johnson, N. L. Rosi, *Chem. Sci.* **2013**, *4*, 1746–1755.
- [15] a) Y. Zheng, L. Lin, X. Ye, F. Guo, X. Wang, *Angew. Chem. Int. Ed.* **2014**, *53*, 11926–11930; *Angew. Chem.* **2014**, *126*, 12120–12124; b) S. Wang, X. Wang, *Angew. Chem. Int. Ed.* **2016**, *55*, 2308–2320; *Angew. Chem.* **2016**, *128*, 2352–2364.

Manuscript received: December 30, 2018

Accepted manuscript online: January 18, 2019

Version of record online: February 7, 2019